Indian J. Res. Found., (2026) 9, 1-3. ISSN 2454-6577

Indian Journal of Research Foundation
An International Multidisciplinary Journal
www.indianjournal.net

RESEARCH ARTICLE

Synthesis and physicochemical characterization of RGO-CuO nanocomposite materials

R. P. Jasmine, M. Vimala Joice *

PG & Research Center of Chemistry, Jayaraj Annapackiam College for Women (Autonomous), Periyakulam -625601, Tamil Nadu, India

Received: 8 June 2026 / Revised: 17 August 2026/ Accepted: 22 September 2026
Corresponding author. E-mail: vjoiceche@annejac.ac.in*

ARTICLE INFO

Keywords

Reduced graphene oxide
Copper oxide
Nanocomposite
Energy storage
Photocatalysis

ABSTRACT

Reduced graphene oxide (rGO)-copper oxide (CuO) nanocomposites were synthesized and characterized to evaluate their structural and functional properties. rGO was prepared by chemical reduction of graphene oxide, while CuO nanoparticles (NPs) were synthesized using a reflux-assisted method. The resulting rGO–CuO nanocomposite was characterized using FT-IR and XRD techniques. The analyses confirmed successful incorporation of CuO nanoparticles onto rGO sheets. The composite exhibited improved structural stability, enhanced surface area, and promising potential for applications in energy storage, catalysis, sensing, and environmental remediation. The synthesized nanocomposite has potential applications in environmental remediation, photocatalysis, energy storage devices, gas sensing, biomedical technologies, and heterogeneous catalysis.

Introduction

Nanotechnology has emerged as one of the most rapidly advancing fields of science and technology due to its ability to tailor the structural, optical, electrical and catalytic properties of materials at the nanoscale [1-3]. Among various nanomaterials, metal oxide semiconductors have attracted significant interest because of their unique physicochemical properties and wide range of applications in catalysis, sensing, energy storage, and environmental remediation. Copper oxide (CuO), a p-type semiconductor with a narrow band gap of ~1.2–1.9 eV, has been extensively investigated owing to its excellent catalytic activity, low cost, abundance, environmental friendliness and high chemical stability.

CuO has found applications in lithium-ion batteries, as sensors, solar cells, photocatalysis, and supercapacitors. However, the practical performance of pure CuO is often limited by its relatively low electrical conductivity, particle agglomeration, and rapid recombination of metal oxides. Among them, graphene and its derivatives have gained tremendous attention due to their exceptional electrical conductivity, high specific surface area, excellent mechanical strength, and chemical stability. To overcome these limitations, carbon-based nanomaterials have been widely employed as supporting matrices for stability. Reduced graphene oxide (rGO), obtained by the reduction of graphene oxide, retains many of the advantageous properties of pristine graphene while offering a cost-effective and scalable route for large-scale production [4]. The presence of residual oxygen-containing functional groups on rGO facilitates the anchoring and uniform dispersion of metal oxide NPs, thereby enhancing the interfacial interaction between the components.

Recently, rGO–CuO nanocomposites have attracted considerable attention because of the synergistic combination of the high electrical conductivity and large surface area of rGO with the catalytic and semiconducting properties of CuO. The incorporation of rGO not only improves electron transport and suppresses NPs agglomeration but also increases the active surface area available for electrochemical and catalytic reactions [5-7]. Furthermore, the strong interaction between CuO NPs and rGO sheets promotes efficient charge separation and transfer, leading to enhanced performance in various applications.

Due to these advantages, rGO–CuO nanocomposites have been widely explored for advanced technological applications such as supercapacitors, lithium-ion batteries, electrochemical sensors, gas sensors, photocatalytic degradation of organic pollutants, wastewater treatment, and antimicrobial materials [8-10]. The improved conductivity, stability, and catalytic efficiency of these composites make them promising candidates for next-generation energy and environmental technologies. In the present work, rGO–CuO nanocomposites were synthesized through a simple chemical route and characterized using Fourier Transform Infrared (FT-IR) spectroscopy and X-ray Diffraction (XRD) analysis. The structural and functional properties of the synthesized materials were investigated to confirm the successful formation of the nanocomposite and to evaluate the interaction between rGO and CuO. The obtained results demonstrate the successful synthesis of rGO–CuO nanocomposites with potential applications in catalysis, sensing, energy storage and environmental remediation.

Experimental

Graphite powder, copper sulfate, sodium hydroxide, and urea were used as starting materials. rGO was synthesized by chemical reduction of graphene oxide using hydrazine hydrate. CuO NPs were prepared through a reflux process involving copper sulfate and urea. The rGO–CuO nanocomposite was obtained by dispersing rGO in water, followed by incorporation of copper precursor and reflux treatment.

Instruments

The IR spectrum was acquired using a SHIMADZU FT-IR Affinity-1 spectrophotometer in the range of 400–4000 cm^{-1}, employing a KBr disc. Powder XRD was carried out using a Miniflex 600 DESKTOP X-ray Diffractometer.

.

Synthesis of reduced graphene oxide

Graphene oxide (50 mg) was dispersed in 50 mL of distilled water and ultrasonicated for 1 h. Hydrazine hydrate was added as a reducing agent, and the mixture was heated at 90 °C for 90 min. The resulting black suspension was washed with distilled water and ammonia solution, centrifuged, and dried to obtain rGO powder [11].

Synthesis of Fe_3O_4 nanoparticles

Copper oxide (CuO) was synthesized. 0.3 g of $CuSO_4 \cdot H_2O$ and 0.6 g of urea were dissolved in 10 mL of double-distilled water in a 100 mL round-bottom flask. To ensure a homogeneous solution, the mixture was stirred for 10 min., before the reaction. The flask was then equipped with a reflux condenser and heated in an oil bath at 90 °C for 6 h under constant magnetic stirring. Following the reaction, the mixture was cooled to ambient temperature, and the resulting precipitate was isolated through filtration. The final CuO product was obtained after drying the precipitate in an oven [12].

Preparation of rGO-CuO nanocomposite

Reduced graphene oxide (rGO, 50 mg, 0.05 g) was dispersed in 50 mL of double-distilled water in a 100 mL round-bottom flask and sonicated for 10 min. to obtain a homogeneous suspension. Subsequently, 0.019 g of $CuSO_4$ and one drop of hydrazine hydrate were added, and the resulting mixture was stirred for 5 min. The reaction mixture was then heated under reflux at 90 °C in an oil bath with continuous magnetic stirring for 1 h. After completion of the reaction, the mixture was allowed to cool to room temperature [13]. The obtained product was separated by filtration, washed thoroughly with double-distilled water, and dried in an oven. The resulting material was collected as the rGO-doped CuO nanocomposite.

Results and Discussion

FT-IR analysis

The FT-IR spectra of the synthesized CuO NPs and rGO–CuO nanocomposite are presented in Figs. 1a,b. A comparative analysis of the spectra confirms the successful incorporation of reduced graphene oxide (rGO) into the CuO matrix. For the CuO NPs as seen in Fig.1, the broad band at 3741 cm^{-1} corresponds to the O–H stretching vibration of surface hydroxyl groups and adsorbed water molecules. The weak peak at 2347 cm^{-1} is attributed to atmospheric CO_2 adsorption. The absorption band at 1647 cm^{-1} is assigned to the bending vibration of adsorbed water molecules, while the band at 1114 cm^{-1} is associated with C–O stretching vibrations of residual oxygen-containing species. The characteristic band at 617 cm^{-1} corresponds to the Cu–O stretching vibration, confirming the formation of CuO NPs [14].

In the rGO–CuO nanocomposite in Fig. 2, the broad band at 3217 cm^{-1} is attributed to O–H stretching vibrations of hydroxyl groups present on the rGO sheets and adsorbed moisture. The band at 2328 cm^{-1} arises from adsorbed atmospheric CO_2. The band at 1635 cm^{-1} corresponds to the skeletal vibration of graphitic C=C bonds and the bending vibration of adsorbed water molecules [15]. The absorption band at 1450 cm^{-1} is attributed to C=C stretching vibrations of the aromatic graphene framework. The band at 1136 cm^{-1} is assigned to C–O stretching vibrations of residual epoxy and alkoxy groups on rGO. The characteristic band at 875 cm^{-1} may be associated with out-of-plane bending vibrations of aromatic C–H groups. Importantly, the characteristic Cu–O stretching vibration is retained at 607 cm^{-1}, confirming the presence of CuO in the composite. Compared with pure CuO, the rGO–CuO nanocomposite exhibits slight shifts in the Cu–O vibration band from 617 to 607 cm^{-1} and the O–H and C–O related bands, indicating strong interfacial interactions between CuO NPs and the rGO sheets. The appearance of additional graphitic carbon-related bands at 1635 and 1450 cm^{-1}, respectively, further confirms the incorporation of rGO into the CuO structure. These spectral changes suggest successful anchoring of CuO NPs onto the rGO surface, leading to the formation of a well-integrated rGO–CuO nanocomposite.

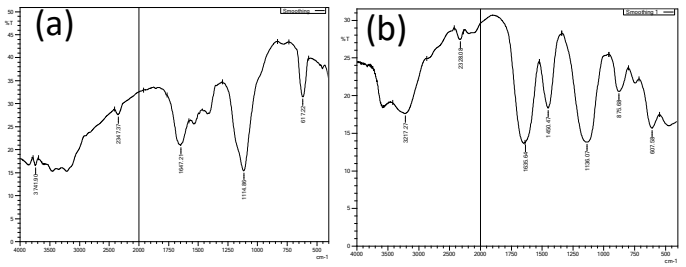


Figure 1. FT-IR spectrum of (a) CuO NPs and (b) rGO–CuO nanocomposite.

The IR results clearly demonstrate the presence of both CuO and rGO characteristic functional groups in the composite. The retention of the Cu–O stretching band along with the appearance of graphitic carbon-related bands and slight peak shifts confirms the successful synthesis of the rGO–CuO nanocomposite and indicates strong interactions between CuO NPs and the rGO matrix. The characteristic IR absorption bands and their corresponding assignments for CuO NPs and the rGO–CuO nanocomposite are summarized in Table 1.

Table 1. Comparison of IR bands of CuO and rGO–CuO nanocomposite.

IR assignments wavenumber (cm^{-1})							
Nanocomposite	v(O–H)	v(CO_2)	v_b(H–O–H)	vs(C=C)	vs(C–O)	v(C–H)	vs(Cu-O)
CuO	3741	2347	1647	-	1114	-	617
rGO–CuO	3217	2328	1635	1450	1136	875	607

XRD analysis

The XRD patterns of the synthesized CuO NPs and rGO–CuO nanocomposite are shown in Figs. 2a,b. The diffraction patterns were analyzed to investigate the crystalline structure and phase purity of the synthesized materials. As seen in Fig. 2a, for the CuO NPs, several diffraction peaks were observed in the 2θ range of 10–90 °, indicating the crystalline nature of the material [16-18]. The prominent diffraction peaks appearing around 32.5, 35.5, 38.7, 48.7, 53.5, 58.3, 61.5, 66.2, 68.1, 72.4, and 75.1° can be indexed to the monoclinic CuO phase. The absence of additional impurity peaks suggests the successful formation of phase-pure CuO NPs. The broadening of the diffraction peaks indicates the nanoscale crystallite size of the synthesized CuO. For the rGO–CuO nanocomposite, the diffraction pattern exhibits characteristic peaks corresponding to CuO along with a broad is illustrated in Fig. 2b.

For the rGO–CuO nanocomposite (Fig. 2b), the diffraction pattern exhibits characteristic peaks corresponding to CuO along with a broad diffraction feature centered around 24–26°, which is attributed to the (002) plane of rGO. The presence of CuO diffraction peaks together with the rGO-related broad peak confirms the successful incorporation of CuO NPs onto the graphene sheets. Compared with pure CuO, slight changes in peak intensity and broadening are observed, which may be attributed to the interaction between CuO NPs and the rGO matrix. The reduced intensity and broadened nature of the rGO peak indicate the exfoliated and partially disordered graphitic structure of reduced graphene oxide [19, 20]. The coexistence of CuO and rGO diffraction peaks in the composite confirms the successful formation of the rGO–CuO nanocomposite without altering the crystalline structure of CuO.

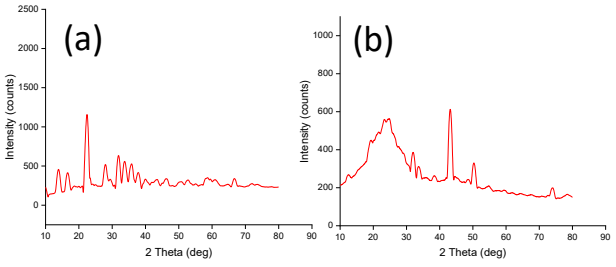


Figure 2. XRD patterns of (a) CuO NPs and (b) rGO–CuO nanocomposite.

The rGO sheets provided a conductive support matrix and prevented nanoparticle aggregation, while CuO NPs enhanced magnetic and redox properties. The synergistic interaction between rGO and CuO contributed to improved structural stability and increased surface area.

Conclusion

The present study successfully synthesized rGO-doped CuO nanocomposites using a simple and cost-effective chemical route. IR results revealed the characteristic Cu–O stretching vibrations along with the functional groups associated with rGO, confirming the successful incorporation of CuO NPs onto the graphene framework. XRD analysis demonstrated the crystalline nature of CuO and the presence of the characteristic rGO diffraction feature, further validating the formation of the rGO–CuO nanocomposite without the generation of secondary impurity phases. The incorporation of rGO into the CuO matrix resulted in strong interfacial interactions between the two components, which can enhance charge transfer, increase surface area, and improve structural stability. The synergistic combination of rGO's excellent electrical conductivity of rGO and CuO's semiconducting properties of CuO is expected to improve the composite's overall physicochemical performance of the composite material. With its enhanced structural, electronic, and surface characteristics, the synthesized rGO–CuO nanocomposite shows significant potential for photocatalysis, electrochemical sensing, energy storage devices, environmental remediation, gas sensing, and other advanced nanotechnology applications. The findings of this study demonstrate that rGO–CuO nanocomposites are promising multifunctional materials for future research and technological development.

References

[1] K.S. Novoselov, A.K. Geim, S.V. Morozov, D. Jiang, Y. Zhang, S.V. Dubonos, I.V. Grigorieva, A.A. Firsov, *Science,* 306 (2004) 666-669.
[2] A.K. Geim, K.S. Novoselov, *Nat. Mater*., 6 (2007) 183-191.
[3] D.R. Dreyer, S. Park, C.W. Bielawski, R.S. Ruoff, *Chem. Soc. Rev*., 39 (2010) 228-240.
[4] S. Park, R.S. Ruoff, *Nat. Nanotechnol.,* 4 (2009) 217–224.
[5] S. Pei, H.M. Cheng, *Carbon*, 50 (2012) 3210–3228.
[6] X. Huang, X. Qi, F. Boey, H. Zhang, *Chem. Soc. Rev*., 41 (2012) 666–686.
[7] M. Ristic, S. Popovic, S. Music, *Mater. Lett*., 58 (2004) 2494–2499.
[8] X. Wang, J. Zhuang, Q. Peng, Y. Li, *Nature*, 437 (2005) 121–124.
[9] Y. Zhao, X. Song, Q. Song, Z. Yin, *Cryst. Eng. Comm.,* 14 (2012) 6710–6719.
[9] Y. Zhao, X. Song, Q. Song, Z. Yin, Cryst. Eng. Comm., 14 (2012) 6710–6719.
[10] K. Zhang, J.M. Suh, T.H. Lee, J.H. Cha, J.W. Choi, H.W. Jang, R.S. Varma, M. Shokouhimehr, *Nano Converg.,* 6 (2019) 6.
[11] W.S. Hummers, R.E. Offeman, *J. Am. Chem. Soc.,* 80 (1958) 1339.
[12] D. Li, M.B. Müller, S. Gilje, R.B. Kaner, G.G. Wallace, *Nat. Nanotechnol.,* 3 (2008) 101–105.
[13] K. Krishnamoorthy, M. Veerapandian, K. Yun, S.J. Kim, *Carbon*, 53 (2013) 38–49.
[14] H. Wang, H.S. Casalongue, Y. Liang, H. Dai, *J. Am. Chem. Soc*., 132 (2010) 7472– 7477.
[15] J. Yan, T. Wei, B. Shao, Z. Fan, W. Qian, M. Zhang, F. Wei, *Carbon*, 48 (2010) 1731– 1737.
[16] H. Bai, C. Li, G. Shi, *Adv. Mater*., 23 (2011) 1089–1115.
[17] M. Pumera, *Chem. Soc. Rev*., 39 (2010) 4146–4157.
[18] A.C. Ferrari, J.C. Meyer, V. Scardaci, C. Casiraghi, M. Lazzeri, F. Mauri, S. Piscanec, D. Jiang, K.S. Novoselov, S. Roth, A.K. Geim, *Phys. Rev. Lett.,* 97 (2006) 187401.
[19] R. Dhineshbabu, V. Rajendran, N. Nithyavathy, R. Vetumperumal, *Appl. Nanosci..* 6 (2016) 933–939.
[20] S. Kumar, A. Kumar, A. Sharma, R. Krishnan, *Mater. Res. Express*, 6 (2019) 1050d8.